THE ANALYSIS OF MECHANISM AND COUNTERMEASURE FOR REDUCING THORACOABDOMINAL INJURY RISK CAUSED BY FAR-SIDE IMPACT

Hitoshi Ida, Yoshito Kusuhara, Masashi Aoki, Michihisa Asaoka
Toyoda Gosei Co., Ltd.
JAPAN

Ning Zhang
Toyoda Gosei North America Corp.
U.S.A.

Shiro Ohara
TGR Technical Center, LLC
U.S.A.

Paper Number 23-0033

ABSTRACT

The European New Car Assessment Programme (Euro NCAP) added requirements in 2020 for the protection of far-side occupants. This is because in a side-impact accident, serious injuries can occur to passengers not only on the near (collision) side but also on the counter-collision (far) side.

Analysis of National Automotive Sampling System/Crashworthiness Data System (NASS-CDS) far-side accidents from 2002 to 2015 revealed that serious injuries occurred not only to the head but also to the chest and abdomen. Liver injury accounts for 48% of all abdominal injuries in occupants with seat belts, and is a type of trauma that must be noted in traffic accident lifesaving.

For head protection, the Euro NCAP test provides criteria for head movement, but no method has been established to quantify liver injury. We attempted to quantify liver injury by simulation using a human body model.

The simulation used the THUMS (Total HUman Model for Safety) human body model in which the shapes of major organs had been modeled. First, the load-displacement characteristics of the liver were modeled from the specimen level to those of the whole organ. Using the liver model, we simulated the behavior of the body in the far-side sled test performed by Pintar et al. [1], and investigated the liver injury index.

We found the maximum principal strain in the liver to range from 60% to 120% in the current model, resulting in laceration of the liver. Using the human body model, we then clarified the injury mechanism of the liver and examined how to reduce injury. In far-side accidents, it was found that the injury was caused by the upper body being catapulted toward the impact side.

A simulation was conducted to determine whether a load on the right side of the occupant to prevent this

sudden and forcible upper body could lessen liver injury.

Simulation results show that the maximum principal strain on the liver can be cut from 120% to 60% by reducing the displacement of the tenth thoracic vertebrae (T10), corresponding to the height of the liver, to within 190 mm on the impact side.

INTRODUCTION

An increasing number of vehicles are installed with side or curtain airbags to protect near-side occupants from side collision from serious injury on collision with another vehicle, a pole or the inside of the car door. A shoulder seat belt can be ineffective, as it tends to disengage from the far-side occupant, and if the occupant moves too far, he or she may be injured by collision with the inside of the car door or with other passengers. It is difficult to protect these far-side occupants with side or curtain airbags, so a different approach is needed for occupant protection than is used for near-side occupants.

For this reason, requirements to protect against far-side accidents were added to the Euro NCAP in 2020. In this test, pole side impact and side impact by AE-MDB (Advanced European Mobile Deformable Barrier) are modeled in sled tests, using WorldSID (World Side Impact Dummy) to evaluate safety in far-side accidents.

The test provides evaluation criteria for head movement, so it is also effective as an indicator of reduction of serious head injury.

In the NASS/CDS survey made by Augenstein et al. [2], 30.5% of chest and abdominal injury sources were identified as due to collision-side interiors, with 22.6% caused by seat belts. However, this data is from 1988 - 1998 and may not be relevant to vehicles manufactured in the 2000s. We therefore newly analyzed far-side accidents using NASS/CDS data from 2002 - 2015 to investigate the effect of seat belts and the patterns of chest and abdominal injuries. These injuries were then reproduced in a simulation model by Ida et al. [3]. This study extended to analyze the mechanisms of injury and to examine countermeasures.

METHODS

Field data analysis

We used the North American Vehicle Accident Database (NASS/CDS) published by NCSA, the statistical control center of NHTSA, in our accident investigation. Injury analysis was conducted on 411 occupants of the driver's seat with AIS 2 or higher injuries and the left side of the second row of ordinary passenger and commercial vehicles involved in far-side accidents over the 13-year period from 2002 to 2015.

Far-side collisions in this report refer to cases of damage to the side of a vehicle in the direction of a collision between 60 - 120 degrees. An analysis of injury tendencies was conducted for occupants taller than 140 cm to evaluate the patterns seen in typical adults. They then analyzed the differences in mortality between occupants wearing and not wearing seat belts, as well as the locations of serious injuries and patterns of abdominal organ injuries.

Development of human body model injury criteria

We developed a simulation model to evaluate liver injury, which frequently occurs in thoracoabdominal injuries caused by far-side accidents.

To analyze the mechanism of liver injury development, we developed a simulation model for liver injury assessment using the THUMS Version 6.1 human body model, which models the structure of the liver.

The approach to developing the simulation model for injury assessment was to first validate the liver material model at the tissue level, then at the whole-organ level, and finally at the whole-body level. (Figure 1)

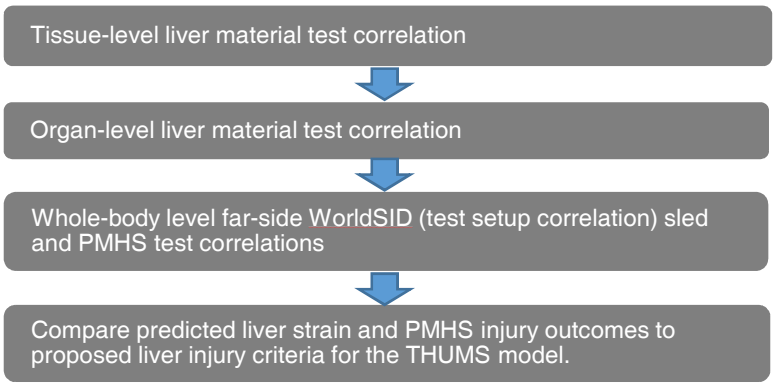

Figure 1. General strategy for human model injury criteria development

Tissue level liver material correlation

Tensile testing of the dog bone-type specimen was simulated using the same element type, size, and hourglass controls as the THUMS liver organ model. The specimen was modeled as 12 mm wide, 40 mm gauge length, and 5 mm thick (Figure 2). Tensile specimens were discretized using a one-node pressure tetrahedral element (LS-DYNA solid element type 13) with an average size of 1 mm. A simplified foam/rubber material model was used to model liver tissue with a bulk modulus of 4.59 MPa, and tensile/compressive material test curves were used to define material behavior. A linear total strain hourglass control (LS-DYNA Type 7) was selected for the solid liver material. A 20 mm stroke was applied to the tensile specimen model over 1 second, producing an approximately 50% engineering strain in the displacement-controlled test mode. The green strain along the tensile direction of the element near the center of the specimen was used as the strain output, the Cauchy stress tensor from the same element was used as the stress output, and the strain-stress curve was then plotted. Strain-stress curves from model simulations were validated against test data [4].

Next, a cylindrical specimen was used to simulate a uniaxial compression material test. Using a symmetric boundary condition, only a quarter of the cylinder was modeled. The specimen was 25.4 mm in diameter and 10 mm in height. A rigid disk was used to apply a 5 mm/s to the specimen, resulting an engineering strain of approximately 50% being applied to the specimen. The friction between the jig and the liver specimen was assumed to be zero. Strain was calculated as engineering strain, and stress was calculated as the contact force in the direction of compression divided by the cross-sectional area. The compressive strain-stress curve from the model simulation was validated against the test data [4].

Finally, to achieve better correlation, the tensile and compressive material curves defining the material properties of the liver were scaled from the current material properties of the THUMS model. The scaled liver material curves were later used for further correlation at the organ and whole-body levels.

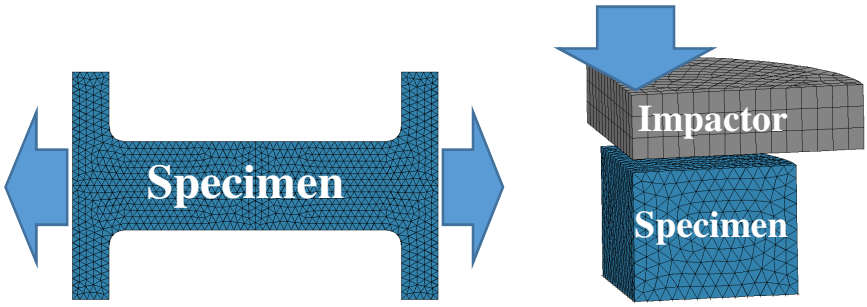

Figure 2. Model shapes of dog bone tensile specimen and cylindrical compressive specimen

Organ-level liver model correlation

The physical properties of the human model were verified using tensile and compression tests of the liver obtained by Kemper et al. from PMHSs (Post Mortem Human Subjects) [4]. A cylindrical impactor with a cross-sectional area of 11.6 cm^2 was impinged on the liver at a constant speed of 200 mm/s (Figure 3). The total stroke of the impactor was 15 mm.

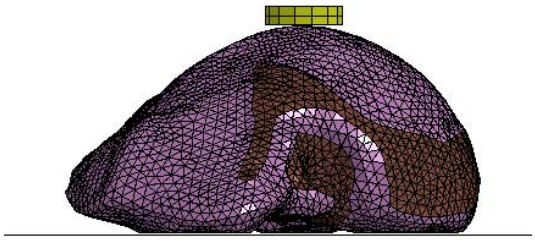

Figure 3. Organ-level liver impactor test setup

Whole-body level correlation

First, the 13 far-side PMHS sled tests performed by Pintar et al. [1] were selected for whole-body level correlation. Test videos and test results were downloaded from NHTSA's Biomechanics Test Database [5].

Second, test fixtures, constraints, and sensor output models were first validated using a test data set from 18 pairs of WorldSID dummies with the same collision severity and constraints as in the PMHS test (Table 1, Figure 4). The WorldSID dummy model from Livermore Software Technology was used. Dummy kinematics, load cell output from the impact wall, and dummy sensor output were verified against the test results. We selected CORA software [6] to quantify the correlation results. CORA's Weight calculated the correlation using a Cross correlation function of 0.667 and Size and Phase shift of 0.167.

Table 1.

Cases used for whole body level correlation. (18 cases selected from the NHTSA biomechanics database to correlate the far-side impact fixture setup; 9 (gray rows) of 18 had a matched pair test with male PMHS.) [I/B: Inboard, O/B: Outboard, PT: Pretensioner]

NHTSA ID	Test ID	Impactor angle	Velocity (m/s)	Shoulder plate	Thorax plate	Seat belt configuration
10158	FSDS107	90	3.25	Yes	No	D-ring at I/B, Low position
10159	FSDS108	90	8.87	Yes	No	D-ring at I/B, Low position
10160	FSDS109	90	8.84	Yes	No	D-ring at O/B, PT
10161	FSDS110	90	3.13	No	Yes	D-ring at I/B, Low position
10162	FSDS113	90	8.69	No	Yes	D-ring at I/B, Low position
10163	FSDS114	90	8.64	No	Yes	D-ring at O/B, PT
10164	FSDS115	90	3.21	No	No	D-ring at I/B, Low position
10165	FSDS118	90	8.92	No	No	D-ring at I/B, Low position
10166	FSDS119	90	8.85	No	No	D-ring at O/B, PT
10167	FSDS121	90	8.57	No	No	D-ring at I/B, Low position, PT
10168	FSDS122	60	3.12	No	Yes	D-ring at I/B, Low position, PT
10169	FSDS123	60	8.20	No	Yes	D-ring at I/B, Low position, PT
10170	FSDS124	60	3.11	No	No	D-ring at I/B, Low position, PT
10171	FSDS126	60	8.47	No	No	D-ring at I/B, High position
10172	FSDS127	60	8.42	No	No	D-ring at I/B, Low position, PT
10174	FSDS130	60	8.13	No	No	D-ring at O/B, PT
10175	FSDS132	90	3.27	No	No	D-ring at O/B, D ring forward
10176	FSDS133	90	8.02	No	No	D-ring at O/B, D ring forward

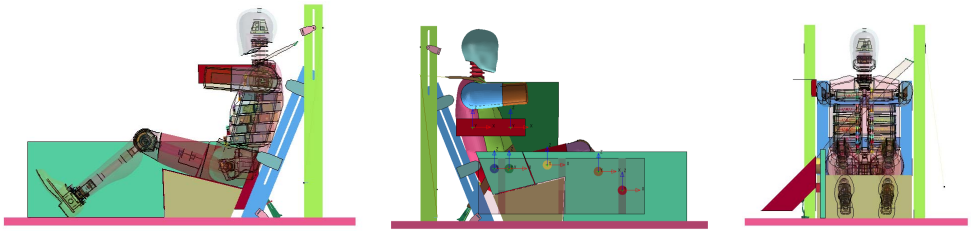

Figure 4. Whole body level far-side sled test setup with WorldSID

Third, the WorldSID dummy model was replaced with a THUMS V6.1 human model, and the impact simulation was repeated to output the kinematics of the human body, deformation of the chest band, rib fractures near the liver, load cell output of the impact wall, and accelerometer output of the first thoracic vertebra (T1), T4,

T12, and the sacrum. CORA scores from these channels were reported for assessment of correlation levels. Thirteen test cases with male subjects close to the 50 percentile physique were reported.

As another set of PHMS tests, simulations were also performed using the 75-degree angle Euro NCAP pulses used in the tests by Petit et al. [7]. The PMHS test by Petit et al., using Euro NCAP pulses, uses the same fixture as the PMHS test by Pintar et al., but the height of the console and the gap between the console and the occupant are different from the test by Pintar et al.

Development of liver injury threshold

After the whole-body correlation had been obtained, the distribution of maximum principal strain (MPS) in the liver was output. Because liver lacerations occur most frequently on the anterior and superior sides of the liver surface [8], elements in these areas were grouped together to obtain time-history curves of strain. Finally, peak strain values and locations were determined. Strain levels were compared to the injury results described in the PMHS autopsy report, and strain values for lacerated liver injuries were derived based on this series of PMHS test data.

RESULTS

Field data analysis

We first analyzed the relationship between using seat belts and injury (Table 2). It was found that occupants who used seat belts had a mortality rate of 18%, while that for occupants not using seat belts was 26%. The average barrier conversion speed of occupants who died using seat belts was 58.66 km/h, while the average barrier conversion speed of occupants who died without seat belts was 42.34 km/h. The results suggest the benefits of seat belt use even in far-side accidents.

Table 2.

Far-side accident occupant data with AIS 2 or higher (survival/death, with or without seat belts)

	With seat belts Survival	With seat belts Death	Without seat belts Survival	Without seat belts Death
Number of Occupants	224	50	101	35
Ave. Age	41.50	43.46	32.88	44.20
Ave. Height	170.04 cm	170.60 cm	172.16 cm	176.06 cm
Ave. Weight	76.15 kg	85.12 kg	84.91 kg	86.37 kg
BMI	26.34	29.25	28.65	27.87
Barrier Equivalent Speed	36.34 km/h	58.66 km/h	32.15 km/h	42.34 km/h
MAIS	2.72	4.52	2.99	4.29
ISS	12.26	40.14	15.82	37.03
Number of injuries	6.53	14.28	8.67	15.20
	Death rate：18%		**Death rate：26%**	

However, because 18% of occupants with seat belts died, we next analyzed the location of AIS4 or higher injuries in occupants with seat belts (Figure 5).

The most common injured body site was to the head, which suggests that the shoulder, whether restrained by a seat belt or kept at the waist, can slip through the seat belt and collide with an interior component on the collision side.

On the other hand, serious injuries to the abdomen, which is relatively close to the waist while being restrained by a seat belt, accounted for 10% of all serious injuries.

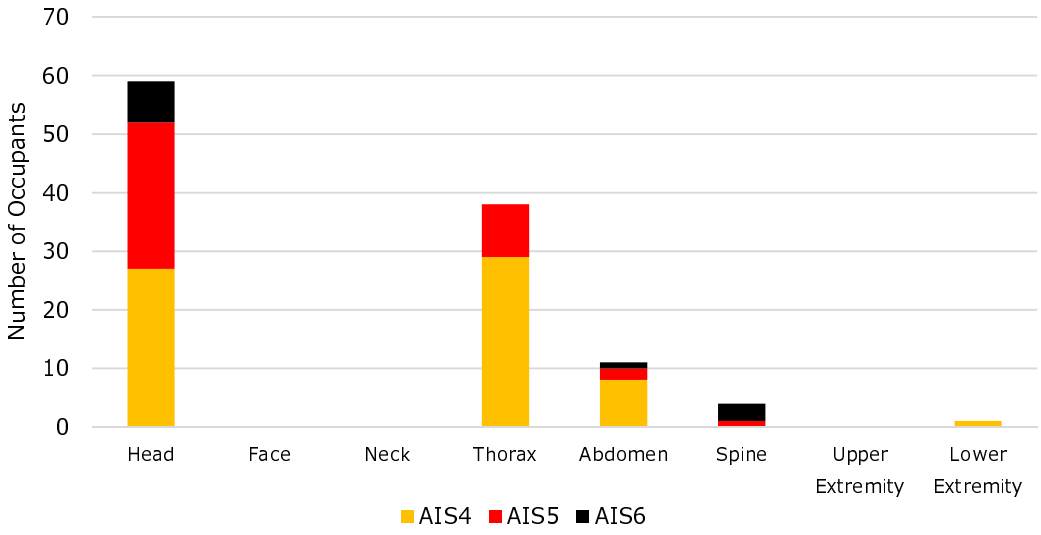

Figure 5. Number of occupants who sustained injuries in far-side accidents of AIS4 or higher with seat belts

Further analysis of the injured organs in the abdominal injuries of occupants with seat belts found that damage to the liver accounted for almost half of the injuries (Figure 6).

Of a total of 53 patients with blunt liver trauma who underwent surgery at the First Affiliated Hospital of the Wenzhou Medical College between 1999 and 2009, 67.9% are reported to have sustained injuries in the right lobe. Major lacerations may be associated with rupture of the right hepatic vein [9].

The superior surface of the liver is attached to the diaphragm by the falciform ligament, suggesting that blunt force to the right side of the right lobe can cause lacerations.

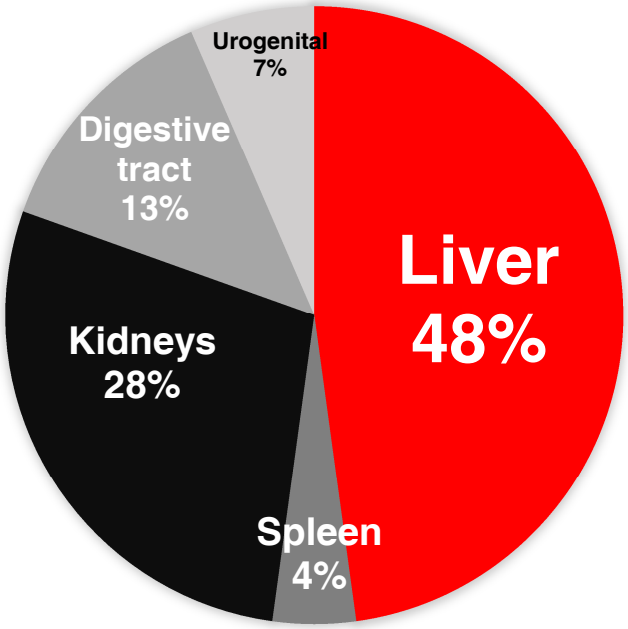

Figure 6. Abdominal organ injury distribution with seat belts (AIS2 or higher)

Development of Human Body Model Injury Criteria

Tissue-level liver material correlation

A simulation model was developed to reproduce the incidence of liver lacerations.

At the tissue level, early THUMS liver material models of THUMS V6.1 were softer than tests showed. Simulations of the material response of the dog bone-type tensile specimens showed the tensile stiffness of the THUMS liver material model to be within the test range but very close to its lower limit. After scaling up the tensile liver material curves by a factor of 1.5, the tensile test results were consistent with the average tensile test data (Figure 7). For compressed material test simulations, the model results were within the test corridor up to 35% of the engineering strain, with the curve close to the lower limit of the corridor. When the load exceeded 35% of the engineering strain, the model results exited the test range and dropped significantly. Based on the

initial results, the stiffness of the liver compression material was scaled up by a factor of four from more than 20% compression strain. After enlarging the compressed liver material curve, the simulated results curve of the compression test remained within the test results corridor (Figure 8). The altered liver material properties were applied to the next steps in organ and whole-body research.

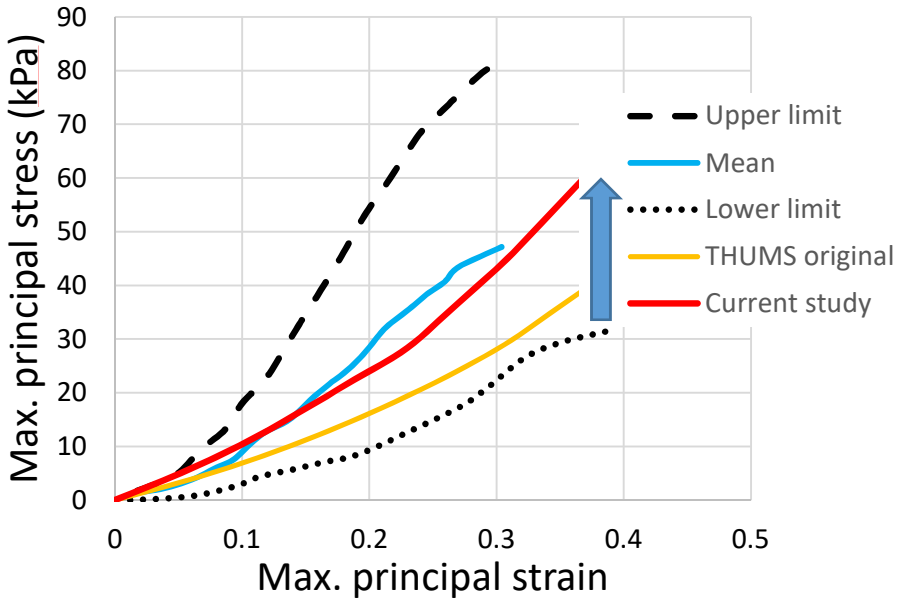

Figure 7. Correlation of liver specimen with tensile tests

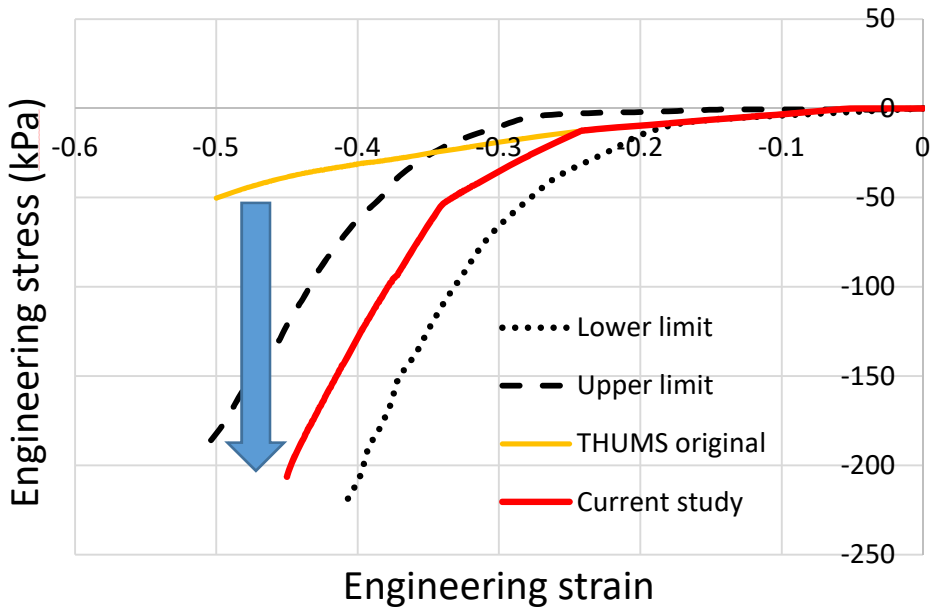

Figure 8. Correlation of liver specimen with compressive test

Organ-level liver model correlation

Simulations were performed using cylindrical impactors at the organ level using physical properties correlated

at the tissue level. The results confirmed that the compression characteristics of the PMHS and those of the simulation model were consistent. (Figure 9)

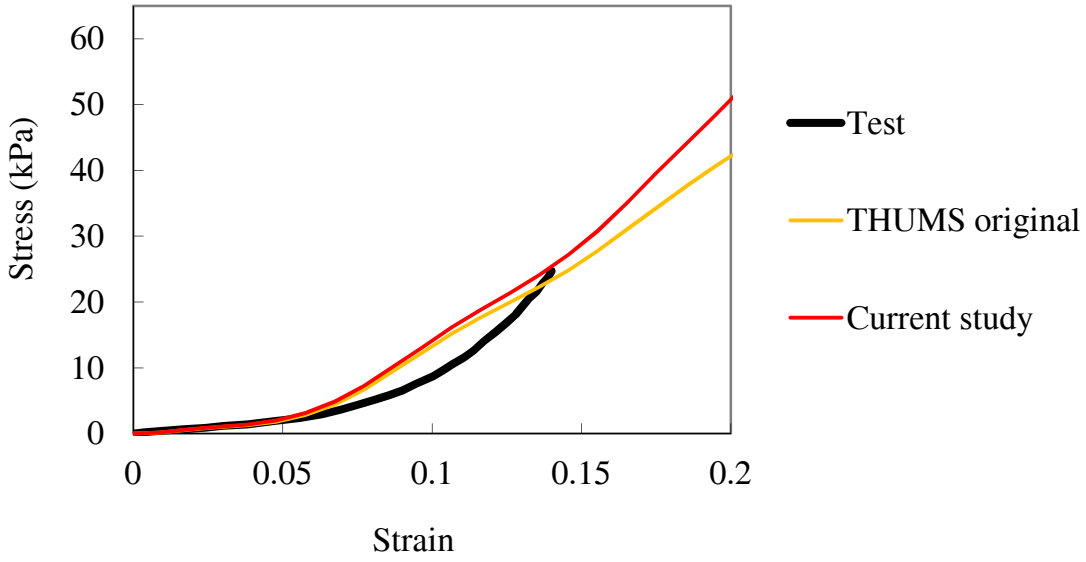

Figure 9. Correlation of liver organ level tests

Whole-body-level correlation

A good kinematic correlation was obtained between the simulation and the test for the WorldSID dummy motion in the sled test by comparing video material (Figure 10, Figure 11). The average CORA score for a total of 18 far-side impact tests was 0.62. The correlation of head acceleration was good. Spinal acceleration correlated well (average CORA score for T1 on Y axis was 0.69, T12 on Y axis was 0.56). Pelvic acceleration correlated well (average CORA score was 0.70 on the y-axis). The correlation level of the load wall force varied according to the location of the load cell (average CORA score for pelvic wall load cells was 0.84, average CORA score for shoulder wall load cells was 0.59).

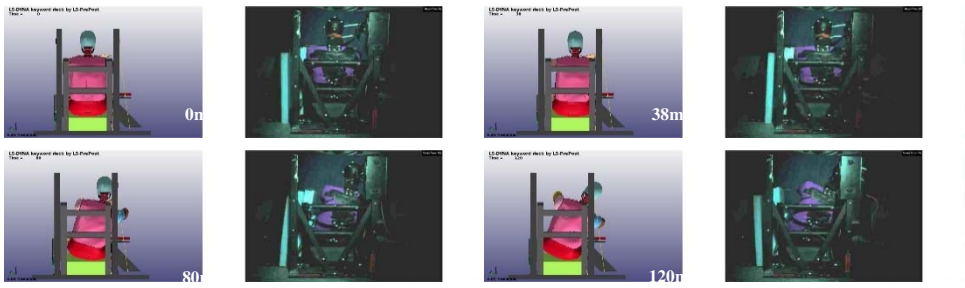

Figure 10. Kinematics comparison between simulation and test videos for WorldSID Case 101

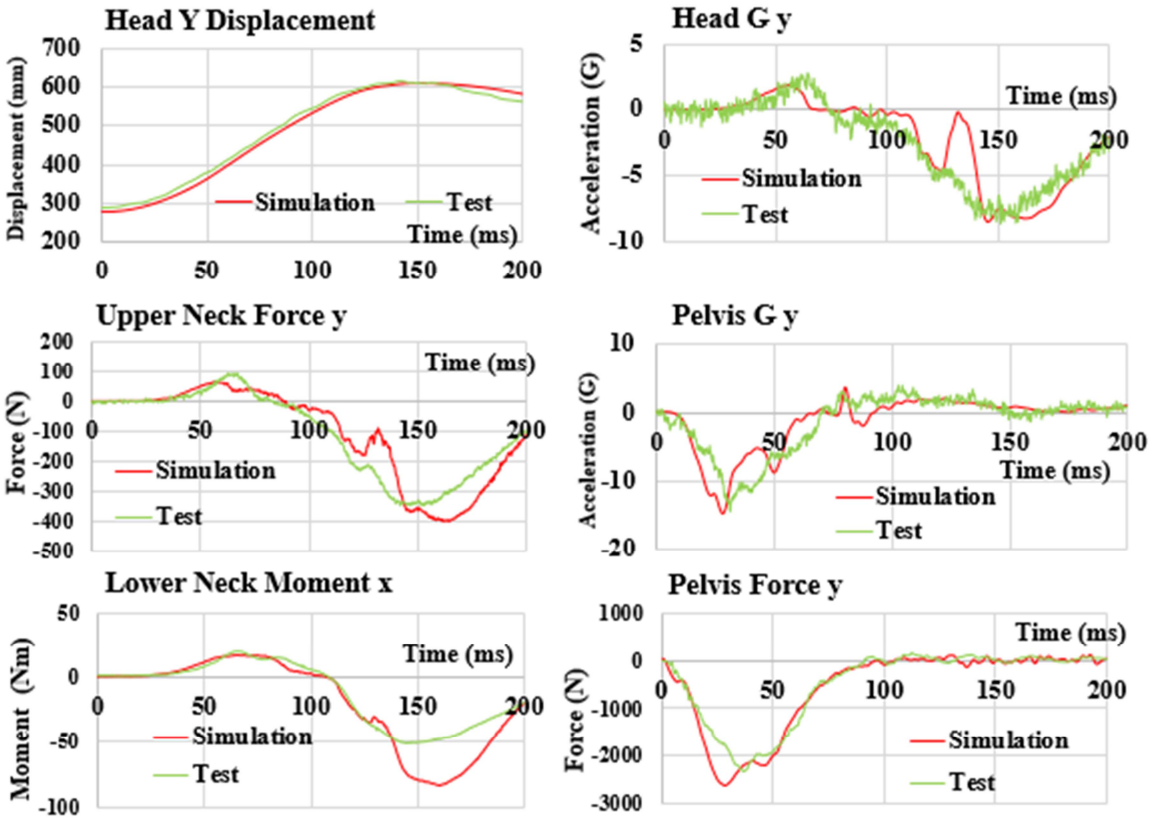

Figure 11. Curve comparison between simulation and test videos for WorldSID Case 10164

The THUMS model of sled simulation yielded good kinematic correlations (The average CORA score for head displacement was 0.92 on the y-axis and 0.65 on the z-axis). Belt force correlation was good (average shoulder belt force CORA score was 0.73). The force correlation of the load wall varied according to the location of the load cell (load cells in the pelvic wall had an average CORA score of 0.82 and load cells in the shoulder wall had an average CORA score of 0.59).

The correlation between rib and spine acceleration was acceptable (mean CORA score was 0.51 for T12 and 0.65 for the sacrum).

Because the rib and spine transducers are noisy, these accelerometers have lower CORA scores (Figure 12). Significant deformation at the lower rib cage level, where it interacts with the console and seat belt, was identified in the simulation (Figure 13), and the deformation of the section in the simulation matched the sled test chest band data corresponding to the height of this console (Figure 14).

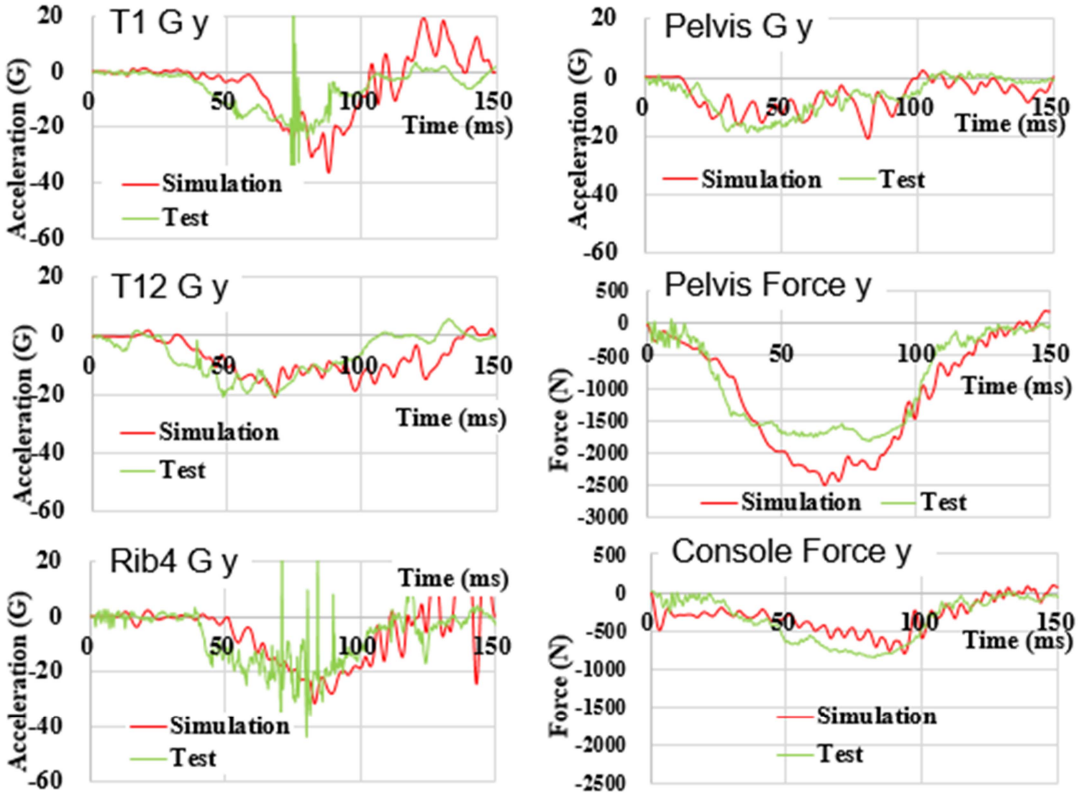

Figure 12. Curve comparison between simulation and test for PMHS Case 10044

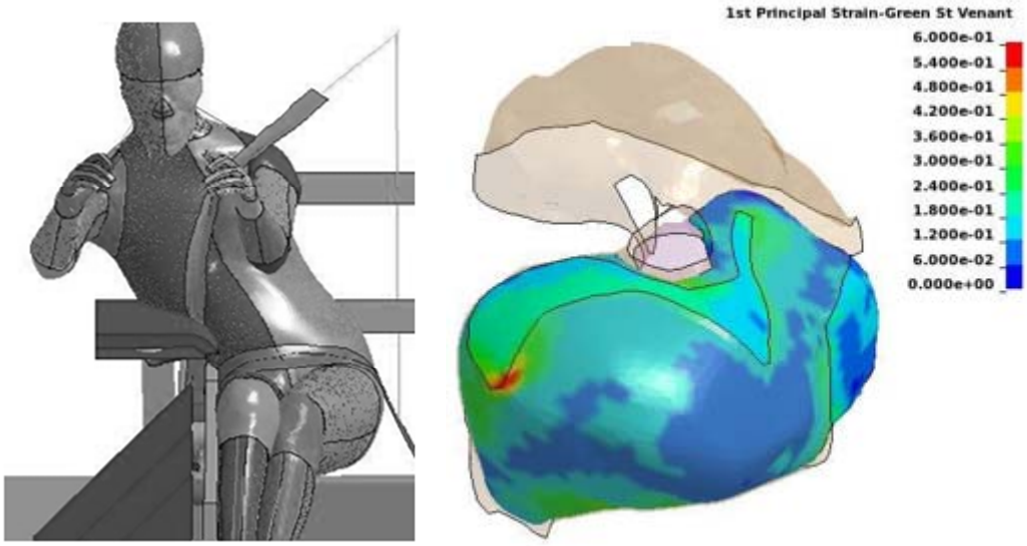

Figure 13. Global kinematics (Left), local liver strain of Case 10045 (Right)

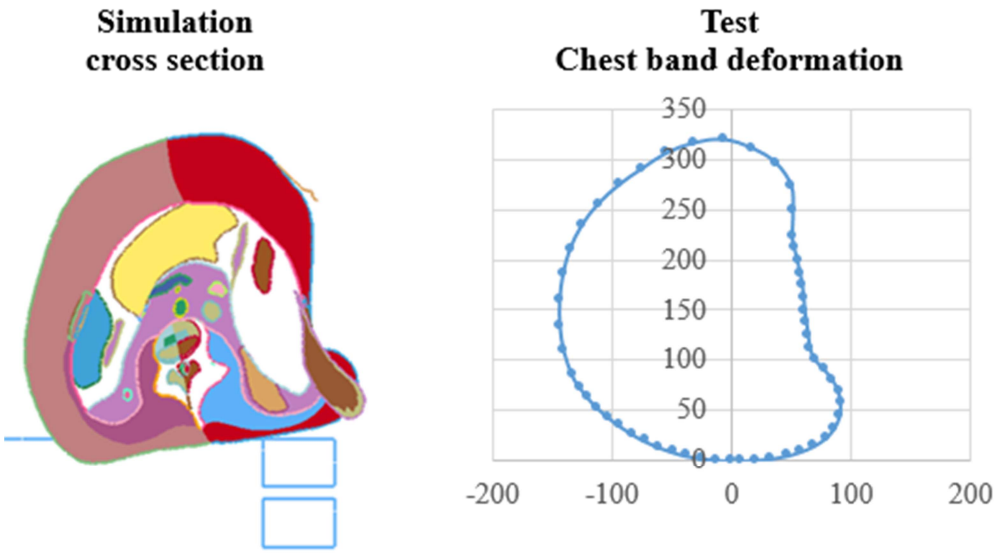

Figure 14. Simulation cross section at console height and chest band deformation from test (Case 10045)

Development of Liver Injury Threshold

Comparison of the maximum principal strain (MPS) of the liver in THUMS mimicking the behavior between studies in which liver lacerations occurred and those in which liver lacerations did not occur confirmed an MPS of 59% in the PMHS study of Pintar et al. [1] and an MPS of 123% in the PMHS study of Petit et al. [7] in which liver lacerations occurred. (Table 3) We assumed an MPS of 60% as the threshold for the risk of liver laceration because the MPS was 28% in cases in which no liver laceration occurred.

In addition, the lateral displacement of tenth thoracic vertebra (T10), which is located at the level of the liver, increased to 249 mm in cases with liver lacerations compared to 188 mm in cases without liver lacerations.

These results suggest that the increased movement of the occupant toward the impact side increases the maximum principal strain in the liver.

Table 3.

Comparison of liver damage between PMHS test and THUMS simulation

PMHS test results			THUMS	THUMS lateral displacement (mm)			
Console height	Test No.	Liver laceration	Liver MPS	Head Y	T1 Y	T10 Y	Pelvis Y
Baseline	10049	No	28%	413	249	188	47
Baseline	10045	Yes	59%	651	451	295	86
Baseline + 50 mm	740	Yes	123%	575	384	249	116

DISCUSSION

Liver injury mechanism

The location of maximum principal strain on the liver surface was the upper surface of the right lobe of the liver where the liver was attached to the diaphragm (Figure15). The reason for the concentration of maximum principal strain here is thought to be that the diaphragm and part of the rib cage moved toward the impact side and pulled the upper surface of the right lobe of the liver that is attached to the diaphragm. The mechanism of this liver injury was also consistent with reports based on clinical data by Jin et al. [9].

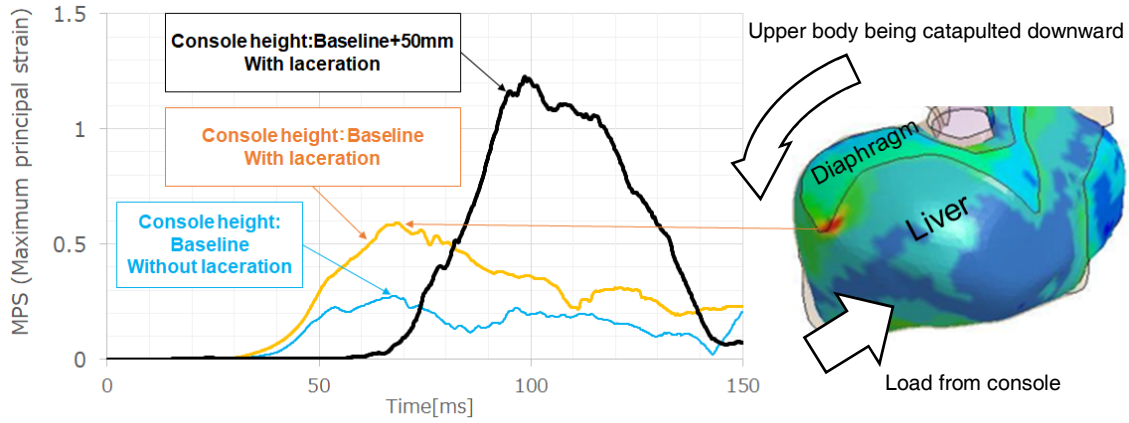

Figure 15. Liver MPS (With/Without laceration)

To confirm the effect of console height on the risk of liver laceration, simulations were performed with the console height increased by 50 mm from baseline. The result showed that when the console height increased by 50 mm, the T10 displacement decreased by 46 mm, but the liver MPS increased more than twice (Table 3). This may be due to the high height of the console, and the lower part of the liver, which receives a blunt impact from the console, could not follow the lateral movement of the ribcage, and the upper surface of the right lobe of the liver attached to the diaphragm may be pulled laterally. (Figure 15, Figure 16).

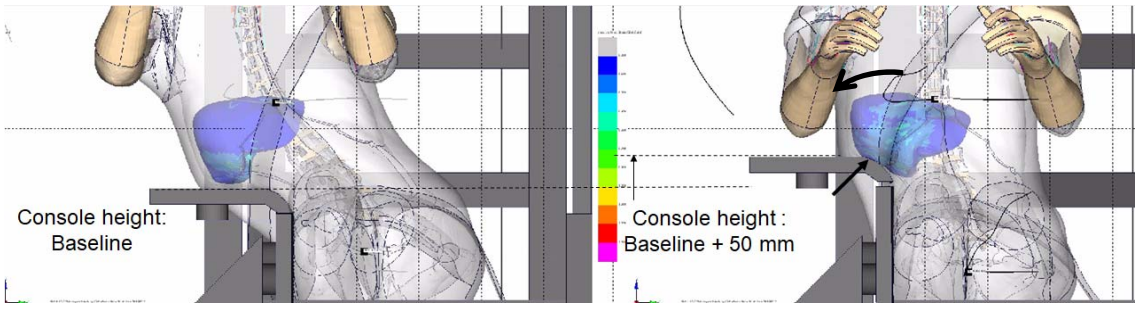

Figure 16. Console height comparison between two simulation cases

In addition, when the console height was increased by 50 mm from baseline, the MPS of the upper surface of

the liver attached to the diaphragm was twice that of the lower surface of the liver that received to blunt force from the console (Figure 17).

These results suggest that it is effective for the protection of abdominal organs to minimize not only the direct external force exerted by the console but also the forced movement of the upper body.

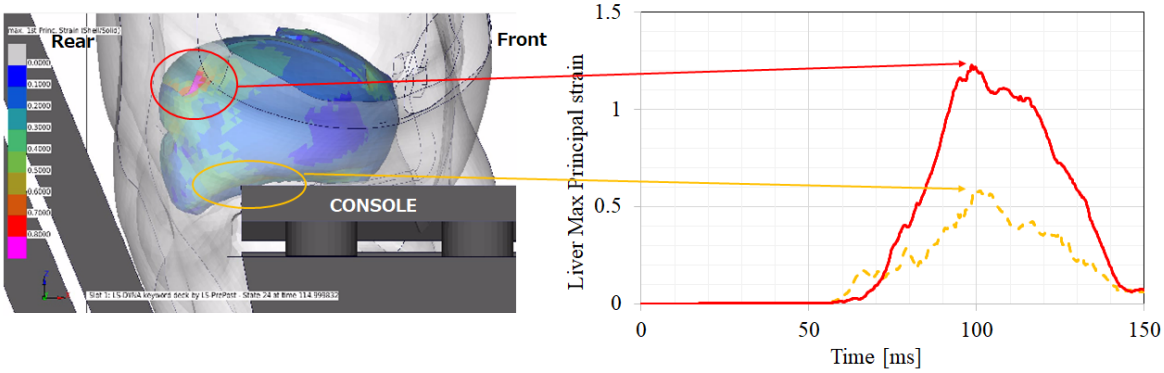

Figure 17. Liver MPS (Upper area/Lower area), Console height: baseline + 50 mm Case

Countermeasures to liver injuries

To confirm the effect of minimizing the forced movement of the upper body, a simulation was performed by applying an external force virtually from the right side of the occupant under the condition of the MPS of the liver being 123% that increased console height 50 mm from baseline (Figure 18).

For the external force from the right, rigid plates covering the occupant's head, shoulders, chest and abdomen, and lower back, which can move only laterally, were placed on the right side. Each rigid plate was given a lateral Force-Displacement characteristic to adjust the movement of the upper body.

As a result of adjusting the movement of T10 to be smaller than in Test No. 10049 without liver laceration as seen in Table 3, the MPS of the liver could be reduced to 55%. (Table 4, Figure 18, Figure 19)

From these results, it was found that to reduce liver injury, it is effective to apply an external force such that the MPS of the liver does not exceed 60% and thus preventing the forced movement of the upper body.

Table 4.

Results of countermeasure

PMHS test results			THUMS	THUMS lateral displacement (mm)			
Console height	Test No.	Liver laceration	Liver MPS	Head Y	T1 Y	T10 Y	Pelvis Y
Baseline + 50 mm	740	Yes	123%	575	384	249	116
Countermeasure (Added lateral force to control body)			55%	317	221	172	114

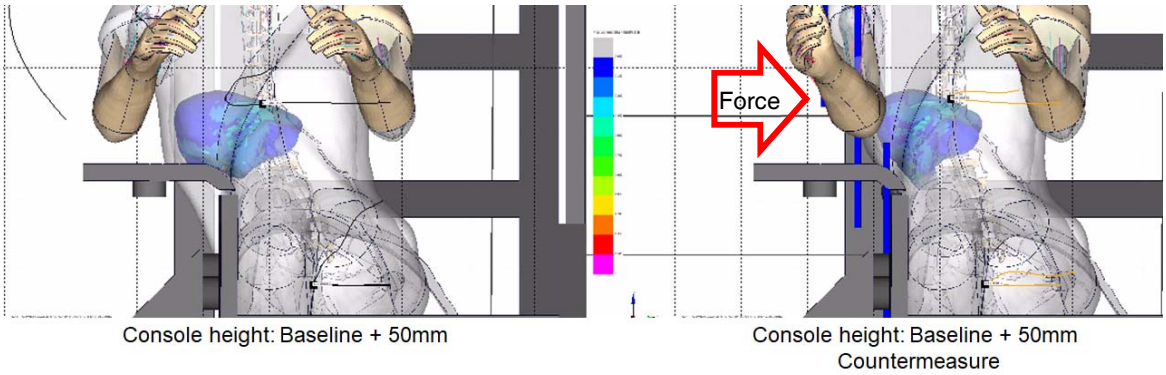

Figure 18. Liver MPS, Console height: Baseline + 50 mm (Left) and Countermeasure (Right)

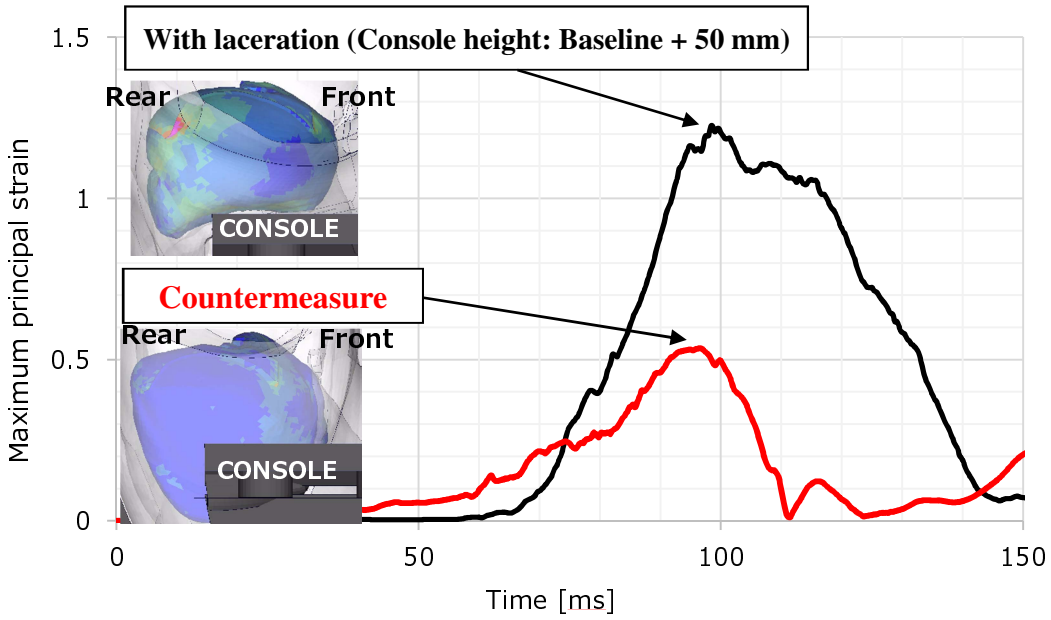

Figure 19. Liver MPS (With laceration / Countermeasure)

CONCLUSIONS

・Analysis of far-side accidents using NASS/CDS accident investigation results showed that 10% of serious injuries to seat belt occupants also included injuries to the abdomen.

・Liver injury accounts for the highest proportion (48%) of abdominal injuries in occupants with seat belts

・To analyze the mechanism of the development of liver injury, a human model THUMS liver was subjected to a donation test.

The behavior of the PMHS sled test was reproduced by checking the material level and the organ alone.

・In the PMHS study, the maximum principal strain (MPS) of the liver of THUMS under conditions where liver laceration occurred exceeded 60%, which was judged to be the threshold for the risk of liver laceration.

・We found that the MPS of the liver was also affected by the height of the console, and that the risk of laceration of the top surface of the liver was likely to increase when the lower end of the liver was loaded by the

console.

・To reduce the risk of liver laceration, it is effective to prevent the forcible movement of the entire upper body.

ACKNOWLEDGEMENTS

The authors would like to thank Dr. Masahito Hitosugi at Shiga University of Medical Science and Mr. Steve Ham at Toyota Technical Center for valuable suggestions and comments.

REFERENCES

[1] Pintar, F., Yoganandan, N., & Stemper, B. (2007). Comparison of PMHS, WorldSID, and THOR-NT Responses in Simulated Far Side Impact. Stapp Car Crash Journal, Vol. 51, 313-360

[2] Augenstein, J., Perdeck, E., Martin, P., Bowen, J., Stratton, J., Horton, T., … Steps, J. (2000). Injuries to restrained occupants in far-side crashes. Association for the Advancement of Automotive Medicine. Vol. 44, 57-66

[3] Ida, H., Aoki, M., Asaoka, M., Zhang, N., Ohara, S., Diederich, A., Hoffmann, J. (2022, November). The development of a thoracoabdominal organ injury index for far-side car occupants exposed to side impacts. Airbag 2022 (15th International Symposium and Exhibition on Sophisticated Car Safety Systems), Mannheim, Germany

[4] Kemper, A., Santago, A., Sparks, J., Thor, C., Gabler, HC., Stitzel, J, & Duma, S. (2011, June). Multi-scale biomechanical characterization of human liver and spleen. 22nd ESV Conference; Washington D.C., USA.

[5] NHTSA, Research Testing Database. (2021). Retrieved from https://www.nhtsa.gov/research-data/databases-and-software

[6] Partnership for Dummy Technology and Biomechanics. (2021). CORA (3.6.1). Retrieved from https://www.pdb-org.com/en/information/18-cora-download.html

[7] Petit, P., Trosseille, X., Uriot, J., Poulard, D., Potier, P., Baudrit, P., Compigne, S., Kunisada, M., & Tsurui, K. (2019, November). Far Side Impact Injury Threshold Recommendations Based on 6 Paired WorldSID /Post Mortem Human Subjects Tests. Stapp Car Crash Journal, Vol. 63, 127-146

[8] Slotta, J.E., Justinger, C., Kollmar, O., Kollmar, C., Schäfer, T., & Schilling, M.K. (2014). Liver injury following blunt abdominal trauma: a new mechanism-driven classification. Surg Today. 44, 241–246.

[9] Jin, W., Deng, L., LV, H., Zhang, Q., & Zhu, J. (2013). Mechanisms of blunt liver trauma patterns: An analysis of 53 cases. Experimental and Therapeutic Medicine. 5, 395–398.